Mathematical Model of the Thermal Processing of Steel Ingots: Part I. Heat Flow Model

B. G. THOMAS, I. V. SAMARASEKERA, and J. K. BRIMACOMBE

A two-dimensional mathematical model has been developed to predict stress generation in static-cast steel ingots during thermal processing with the objective of understanding the role of stress generation in the formation of defects such as panel cracks. In the first part of a two-part paper the formulation and application of a heat-flow model, necessary for the prediction of the temperature distribution which governs thermal stress generation in the ingot, are described. A transverse plane through the ingot and mold is considered and the model incorporates geometric features such as rounded corners and mold corrugations by the use of the finite-element method. The time of air gap formation between mold and solidifying ingot skin is input, based on reported measurements, as a function of position over the ingot/mold surface. The model has been verified with analytical solutions and by comparison of predictions to industrial measurements. Finally, the model has been applied to calculate temperature contours in a 760 × 1520 mm, corrugated, low-carbon steel ingot under processing conditions conducive to panel crack formation. The model predictions are input to an uncoupled stress model which is described in Part II.

I. INTRODUCTION

STEEL ingots are subject to many defects that arise during processing as a consequence of metallurgical weaknesses in combination with stress generation. One such defect is panel crack formation which affects aluminum-treated, plain carbon steel ingots over a range of compositions and ingot sizes. The loss of ductility in steel at intermediate temperatures, which is partly responsible for the problem, has received a great deal of study which was reviewed in a previous paper.[1] However, the generation of stresses in ingots, which is also a great contributor to the problem,[2] has received relatively little attention.

The stress generated in a static-cast ingot during processing prior to rolling is caused almost entirely by the volumetric expansions and contractions accompanying changing thermal gradients within the ingot. As the first step in calculating these stresses, it is therefore important to determine accurately the internal thermal state of the ingot as a function of time. Thus, the objective of the first part of this work was to develop a mathematical model to calculate the temperature distribution in a steel ingot as a continuous process from the end of teeming to the start of rolling, including solidification, cooling in the mold and in air, reheating in the soaking pit, and subsequent air cooling.

Many mathematical heat-transfer models of static-cast ingot processing have been documented and used in recent years.[3–15] However, relatively few of the models were designed with subsequent thermal stress modeling in mind, and no model reported in the literature has yet been utilized to study panel cracking. Most previous models have been formulated using a finite-difference method and have modeled the ingot as a square or rectangle.[3–5,7–11,15] While this approximation can be used effectively to predict total solidification time,[3,7–9,15] the actual temperature fluctuations, important to stress generation, are more sensitive. Since the importance of mold corrugations on stress development was not known, the present model was formulated using a version of the finite-element method in order to simulate the exact geometry including the effects of rounded corners and mold corrugations.

In a later paper, both the heat-flow and stress models will be applied to elucidate the mechanisms behind panel crack formation. Thus, a number of assumptions made in the formulation of both models reflect this end use. In particular, the steel compositions, physical and mechanical property data, ingot size, and processing conditions employed are all chosen to simulate conditions conducive to panel cracking.[2]

II. MODEL FORMULATION

Panel cracks are predominantly longitudinal in the central regions of the ingot. Indeed, they usually appear first near the center and extend upward and downward only in severe cases. Thus, for the model, only two-dimensional heat flow in a transverse section through the mid-height of the ingot is considered, wherein the essential features of panel crack formation should be revealed. The inaccuracies associated with this assumption are slight since the heat transmitted from the top and bottom of the ingot is small and nearly symmetrical.[3,7,9] The benefits are a substantial saving in computer costs and ease of analysis of results.

Another simplification that can be made is two-fold symmetry about the mid-planes in the transverse section. Such symmetry is actually exhibited by the panel cracks themselves and requires that only one-quarter of the transverse section be modeled.

The governing equation for heat conduction within the steel ingot and cast iron mold is then:

$$\frac{\partial}{\partial x}\left(k\frac{\partial T}{\partial x}\right)+\frac{\partial}{\partial y}\left(k\frac{\partial T}{\partial y}\right)=\rho C_p\frac{\partial T}{\partial t} \qquad [1]$$

B. G. THOMAS, formerly a Graduate Student at the University of British Columbia, is Assistant Professor in the Department of Mechanical and Industrial Engineering, University of Illinois, 1206 West Green Street, Urbana, IL 61801. I. V. SAMARASEKERA, Associate Professor, and J. K. BRIMACOMBE, Stelco/NSERC Professor and Director, are with The Centre for Metallurgical Process Engineering at the University of British Columbia, Vancouver, BC, Canada, V6T 1W5.

Manuscript submitted February 3, 1986.

Since the initial stages of solidification are known to be of lesser importance to panel cracking, a number of other simplifying assumptions were made.

1. Teeming was assumed to take place instantaneously, thus allowing the initial condition to be liquid steel at a constant temperature. To account partially for cooling during teeming, values were chosen to be approximately 10 °C lower than average initial casting temperatures found industrially. The mold was initially assumed to be at a uniform, ambient temperature.
2. Convection in the liquid pool was ignored. Calculations showed that varying convection from stagnant to well stirred by artificially raising the thermal conductivity of liquid steel made very little difference to the subsequent temperature distributions and only introduced uncertainties in the location of the liquidus front, which is of relative unimportance to the present problem. The temperature-dependent functions for the thermal conductivities of steel and cast iron that were used in the model are illustrated in Figure 1. The function for steel was established by compiling data from several different sources[16,17] and includes a dependence on carbon content. The function for cast iron has been used in previous models.[6,13]
3. The latent heat of solidification (272 kJ/kg) was assumed to evolve linearly over the two-phase region between the liquidus, T_{LIQ}, and solidus, T_{SOL}, temperatures. Figure 2 illustrates the temperature-dependent functions for the heat contents of steel and cast iron which were used in the heat-flow model. The enthalpy functions also were based on data from several different sources for steel[6,16–18] and cast iron.[6,13,19]
4. Density variations were ignored since they are mainly due to thermal contraction, and with nonvariable mesh dimensions, maintaining constant mass is more important.[3,7] Constant densities of 7400 kg/m^3 for steel and 7100 kg/m^3 for cast iron were assumed.
5. Any effects of segregation on the thermal properties were ignored so that the same data could be applied throughout the ingot.
6. Any effects of heat transfer through the scale layer on the ingot surface during reheating or subsequent cooling were ignored.

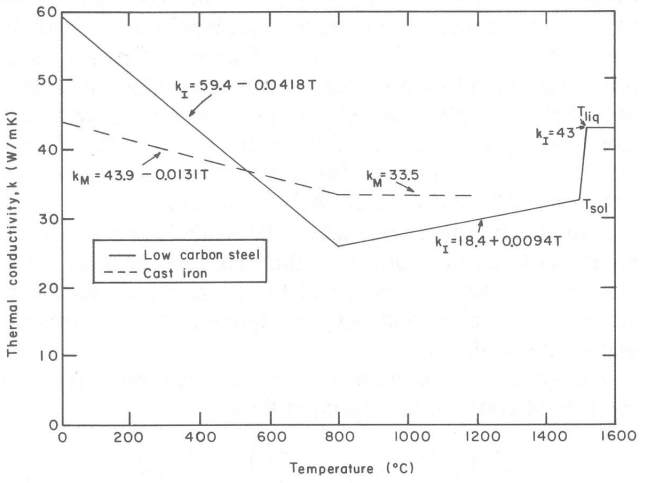

Fig. 1—Thermal conductivity functions for steel and cast iron used in heat-flow model.

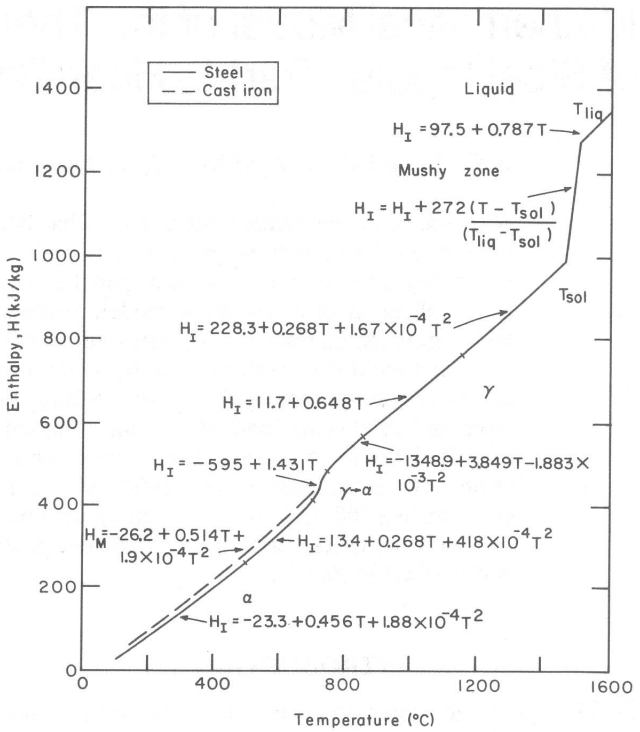

Fig. 2—Enthalpy functions for steel and cast iron used in heat-flow model.

7. Liquidus and solidus temperatures were determined from input composition data using the empirical relations:

$$T_{LIQ} = 1537 - 88\,(\text{pct C}) - 25\,(\text{pct S}) - 5\,(\text{pct Cu}) - 8\,(\text{pct Si}) - 5\,(\text{pct Mn}) - 2\,(\text{pct Mo}) - 4\,(\text{pct Ni}) - 1.5\,(\text{pct Cr}) - 18\,(\text{pct Ti}) - 2\,(\text{pct V}) - 30\,(\text{pct P}) \quad [2]$$

$$T_{SOL} = 1535 - 200(\text{pct C}) - 12.3(\text{pct Si}) - 6.8(\text{pct Mn}) - 124.5(\text{pct P}) - 183.9(\text{pct S}) - 4.3(\text{pct Ni}) - 1.4(\text{pct Cr}) - 4.1(\text{pct Al}) \quad [3]$$

These equations were adopted from existing literature.[20,21]

III. BOUNDARY CONDITIONS

The boundary conditions for ingot processing prior to rolling are divided into four separate temporal regions corresponding to:

1. Solidification and cooling in the mold during the "jacketed time",
2. Ambient air cooling during the "unjacketed time",
3. Reheating in the soaking pit, and
4. Ambient air cooling after removal from the soaking pit.

The boundary conditions are also divided into four distinct spatial segments. These are the ingot centerplanes, ingot exterior, and mold interior or the ingot/mold "gap", and the mold exterior. They are illustrated in Figure 3 for a one-quarter transverse section at mid-height through an ingot and mold chosen to represent a typical geometry affected by off-corner panel cracks.

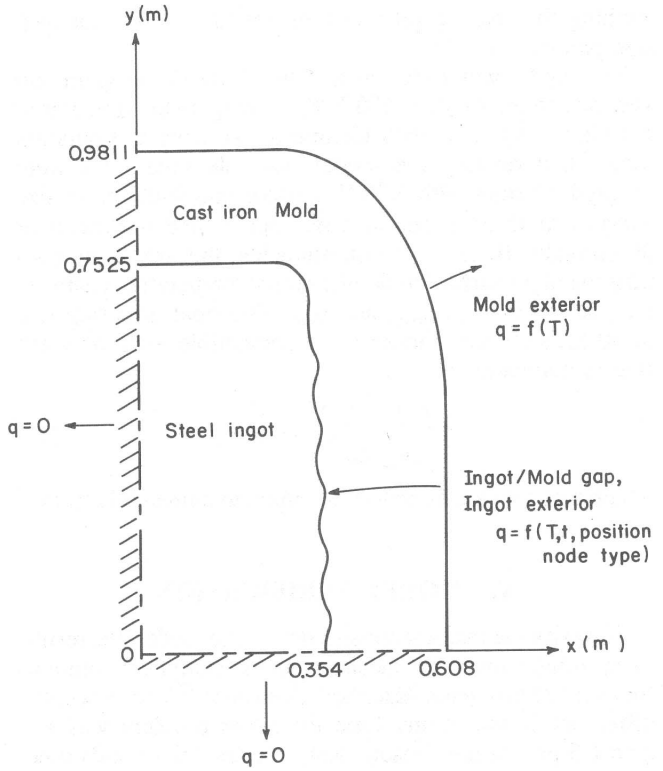

Fig. 3—One-quarter transverse section through a 760 × 1520 mm ingot (originally exhibiting an off-corner panel crack[27]) considered in the heat-flow model.

Generally, the boundary conditions can be expressed mathematically as follows:

$$t > 0, \qquad -k\frac{\partial T}{\partial x} = q \qquad [4]$$

or

$$t > 0, \qquad -k\frac{\partial T}{\partial y} = q \qquad [5]$$

Throughout the thermal process, the two-fold symmetry assumed is imposed mathematically by setting $q = 0$ at the ingot centerplanes.

A. *Mold Cooling*

The first stage of ingot processing requires the inclusion of the mold into the model. Conduction is the only mode of heat transfer within the ingot and within the mold. Heat is lost from the exterior surface of the mold through radiation and natural convection to the surroundings at ambient temperature

$$t < t_{strip}, \qquad q = \sigma\varepsilon_M(T_{SM}^4 - T_\infty^4) + 1.24(T_{SM} - T_\infty)^{1.33} \qquad [6]$$

The second term of this equation was based on an empirical relationship for natural convection for turbulent flow over vertical plates[22] and produces heat-transfer coefficients of the order of 10 W/m^2 K.

Between the ingot and the mold, heat initially flows by conduction; but after a short time the ingot shrinks away from the mold, giving rise to an air gap. This gap is sufficiently large that conduction through the air is unimportant and radiation becomes the dominant mode of heat transfer. Several workers have investigated heat transfer across the mold-ingot interface during the initial stages of solidification.[15,23–25] The time of gap formation, t_{gap}, was found to increase significantly with increasing distance from the corner. Many previous models have assumed instantaneous gap formation[4,5,7,8] but, ignoring the high rates of heat conduction that occur prior to gap formation, was found to produce significant errors in temperature prediction,[15] particularly for large ingots where the gap formation time may exceed 1500 seconds (25 minutes) at the middle of the broad face.[25] Thus for the present model, a relationship based on the data from Oeters,[25] shown in Figure 4, was developed:

$$t_{gap}(s) = 50 + 10{,}800[d(m)]^{1.6} \qquad [7]$$

The heat transferred from the ingot exterior to the mold interior during this stage was taken to be the larger of

$$q = h_{cond}(T_{SI} - T_{SM})$$

$t < t_{strip}$,

$$q = \sigma\bar{\varepsilon}(T_{SI}^4 - T_{SM}^4) \qquad [8]$$

where the conductive heat-transfer coefficient, h_{cond}, was assumed to drop linearly from an initial maximum of 1700 W/m^2 K to zero at t_{gap}. The effective emissivity, $\bar{\varepsilon}$, for radiant exchange between parallel plates is given by[26]

$$\bar{\varepsilon} = \frac{1}{\frac{1}{\varepsilon_I} + \frac{1}{\varepsilon_M} - 1} \qquad [9]$$

and typical values for ingot and mold surface emissivities were taken to be $\varepsilon_I = 0.9$ and $\varepsilon_M = 0.85$.

B. *Air Cooling*

In the second stage, after the ingot has been stripped from the mold, heat is lost directly from the ingot surface to the ambient surroundings by radiation and natural convection according to

$t_{strip} < t < t_{track}$,

$$q = \sigma\varepsilon_I(T_{SI}^4 - T_\infty^4) + 1.24(T_{SI} - T_\infty)^{1.33} \qquad [10]$$

The fourth stage of air cooling, which corresponds to removal of the ingot from the soaking pit, ($t > t_{draw}$), can be treated in a similar manner.

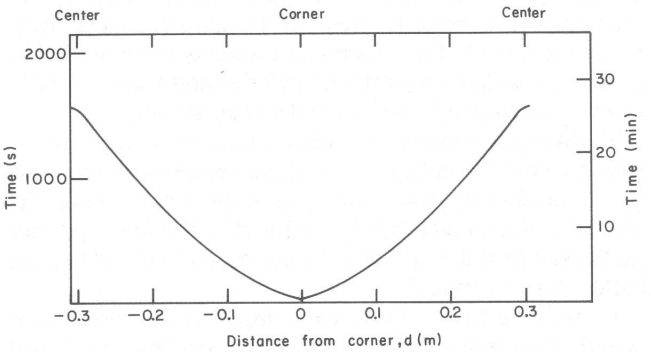

Fig. 4—Air gap formation times halfway up mold for a 6 ton, 600 mm square ingot.[25]

C. *Soaking Pit Reheating*

During the third stage, the ingot gains heat by radiation and forced convection in the soaking pit. Since previous calculations have shown that the heat transferred by forced convection in a bottom-fired soaking pit, with which the present study was most concerned, is small, this term was ignored.[27] A simplified model for heat flux to the exterior surface of the ingot during this complex soaking stage was, therefore, adopted:

$$t_{track} < t < t_{draw}, \qquad q = \sigma \varepsilon_I (T_{PIT}^4 - T_{SI}^4) \qquad [11]$$

where the average interior pit temperature, T_{PIT}, was input as a function of time according to the designed reheating schedule. This function was defined in terms of the initial pit temperature, high firing time, equilibrium soaking temperature, and soak time to permit the simulation of a wide variety of soaking pit reheating conditions.[27] Aside from the mold geometry and steel composition, the only controllable variables for ingot processing were assumed to be t_{strip} and t_{track} and the soaking pit reheating schedule.

All of the events in the processing of the ingot used by the model, such as the strip time, t_{strip}, and the track time, t_{track}, refer to the time interval since initial casting of the steel.

IV. SOLUTION TECHNIQUE

The results of a previous comparison of numerical simulation techniques[28] indicated that this type of transient heat-conduction problem, involving irregular mold geometry, can be solved most effectively using the finite-element method. The optimum technique described in the previous study was determined to be the matrix version of the finite-element method[29] using three-node, linear-temperature, triangular elements, coupled with the Dupont three-level, time-stepping scheme,[30,31] specified heat-flux (Neumann) lumped, boundary conditions formulated with property evaluation at the second time level,[28] and the Lemmon technique[32] for handling latent heat evolution. A computer program based on this method was developed to solve for the temperature distribution in the ingot and mold using the previously described boundary conditions. A flowchart describing the program is given in Figure 5.

The ingot and mold regions were discretized separately into meshes of three-node, linear-temperature, triangular elements as mentioned earlier. A computer plot of the elements was obtained to verify that the program was correctly generating the mesh data. Initial runs with both coarser and finer meshes were conducted before optimum mesh sizes were determined. The meshes of elements were graded to include extra detail near the boundaries and were carefully constructed to avoid angles greater than 90 deg.

To distinguish the ingot surface from the mold surface at their common boundary, two different nodes with the same (x, y) coordinates were employed at each point along the interface. Each node that formed part of the ingot exterior exchanged heat directly with its corresponding node on the mold interior surface.

In addition to the mesh data, input to the model also included the initial temperatures of the cast-iron mold and molten steel, steel compositions (with which to calculate thermal property data), strip time, track time, function describing the soaking pit reheating schedule, and time-step size parameters.

The model was coded as a FORTRAN IV program and was run on an Amdahl 470 V/8, 12-megabyte computer at the University of British Columbia. To save computation time when running the model, variable time steps were adopted, starting with 0.9375 seconds and doubling in size every 4 to 15 iterations to a maximum time increment of 30 seconds. To minimize inaccuracies, this was done each time the ingot surface underwent rapid temperature changes, *i.e.*, at $t = 0$, t_{strip}, t_{track}, and t_{draw}. The final time step size of 30 seconds was chosen to be compatible with the mesh size in maintaining

$$\left(\frac{k}{\rho C_p}\frac{\Delta t}{\Delta x^2}\right) \approx 0.1 \qquad [12]$$

which was previously found to minimize numerical errors.[28]

V. MODEL VERIFICATION

To verify the internal consistency of the model, the results from initial runs were checked against analytical solutions for two test problems described elsewhere.[27] The maximum difference found at any time for either problem was less than 1.5 pct for the chosen mesh size and 30-seconds time-step size.

The model then was formulated to calculate temperatures for comparison with experimental measurements. The first simulated the solidification of a small, 230 × 405 mm (9 × 16 in.) steel ingot cast at Stelco for experimental temperature measurement.[33] A mesh, shown in Figure 6, was generated to match the dimensions of the ingot mold. An initial steel teeming temperature of 1620 °C was input together with T_{LIQ} = 1527 °C and T_{SOL} = 1515 °C. Figure 7 compares the temperatures predicted by the model with those measured at the exterior surfaces of the mold. The temperature predictions are in general close (within 10 pct) but are consistently slightly high. This is likely due to the fact that the thermocouples used to measure the mold temperatures were positioned well above mid-height where axial heat conduction was significant.

The second simulation compared model predictions with temperature measurements conducted by Behrens and Weingart[34] on a larger, 870 × 1130 mm, 15,000 kg steel ingot. The same mesh shown in Figure 6 was employed in this analysis by distorting it to match these dimensions. The initial temperatures and steel property data input are given in Table I. Figure 8 illustrates the striking qualitative agreement between predicted and measured temperature histories at the exterior surface of the ingot at the center of the broadface in the ingot/mold gap. The agreement is consistently within 5 pct. Of particular interest is the presence in both the theoretical and experimental analysis of a rapid drop followed by a temporary rise in temperature. The dotted portion of the experimental curve represents an estimated average of fluctuating temperatures as the solidifying shell formed an unstable air gap.[34] Stable air gap formation was accompanied by reheating of the ingot surface which will be elaborated on later. Finally, the predicted time for complete solidification of 15,900 seconds (4.4 hours) compares closely with the experimentally estimated time of 16,500 seconds (4.6 hours).

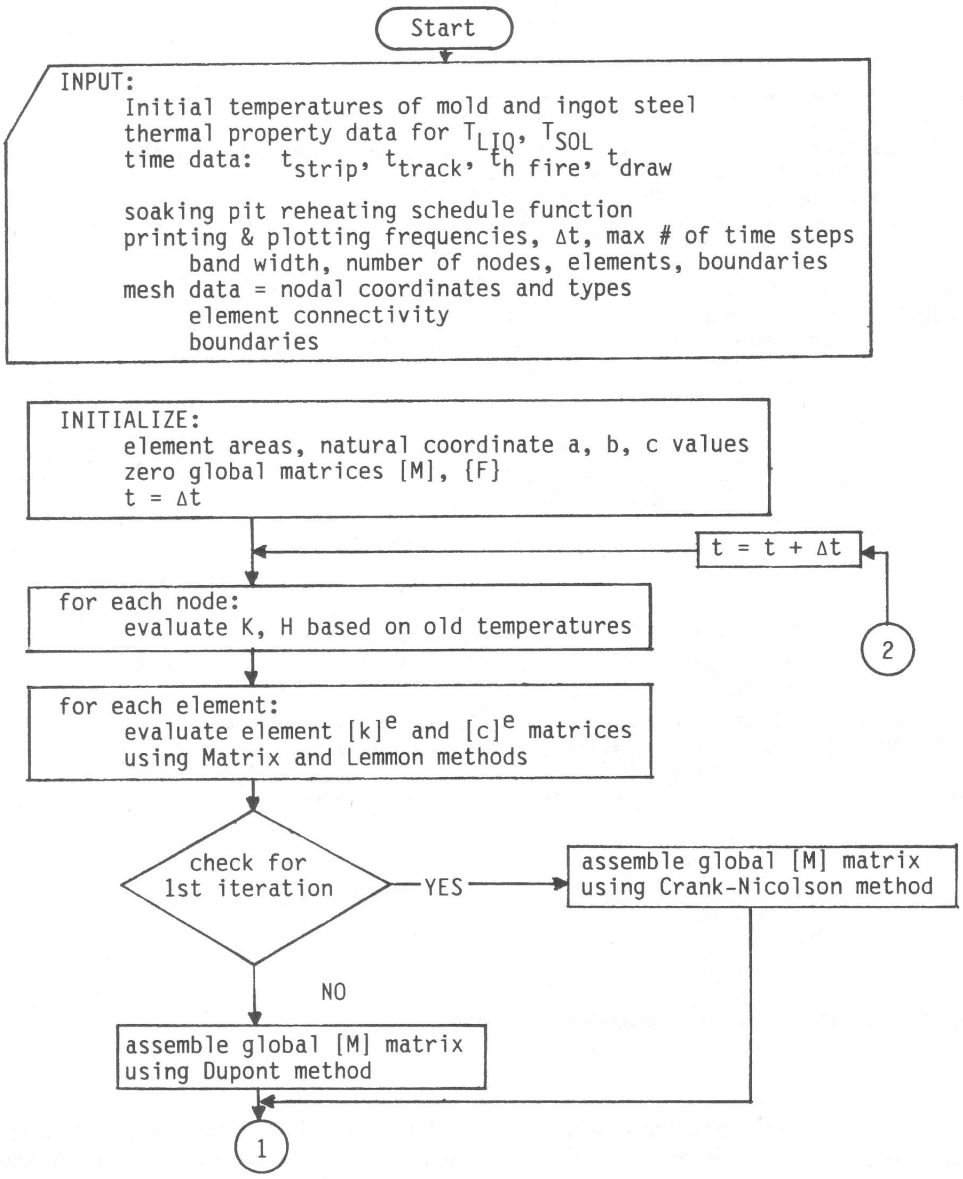

Fig. 5—Flowchart of finite-element heat-flow model computer program.

In conclusion, the heat-transfer model was judged to predict temperatures in a steel ingot during processing to a reasonable degree of accuracy. This is significant since the only adjustable parameters used in the model are directly linked to measurable process variables.

VI. SENSITIVITY ANALYSIS

To determine the relative importance of various model parameters, a sensitivity analysis was performed on the heat transfer model. The runs simulated solidification in the mold of the 230 × 405 mm test ingot, and for convenience, the total solidification time was used as the means for comparison. The results are as follows:

1. Using a rectangular mesh without corrugations increased solidification time by 20 pct over that obtained for a curved, corrugated mesh.
2. Increasing the mold wall thickness by 5 pct for the same ingot size initially produced a 13 pct decrease in solidification time. Continued increasing of the mold wall thickness eventually increased the solidification time; however, the overall decrease in the rate of heat conduction through the mold wall ultimately overcame the increased heat-sink effect.
3. Using constant 60-second time steps instead of finer, variable time steps decreased solidification time by about 800 seconds. For the small test ingot, this represents a 40 pct reduction. However, the absolute time reduction was relatively independent of ingot size, so the effect is much less for larger ingots.
4. Using a coarser mesh (containing one-quarter as many nodes) reduced solidification time by 10 pct.
5. Increasing both the ingot and mold size by 30 pct in cross-sectional area resulted in a 25 pct increase in solidification time.

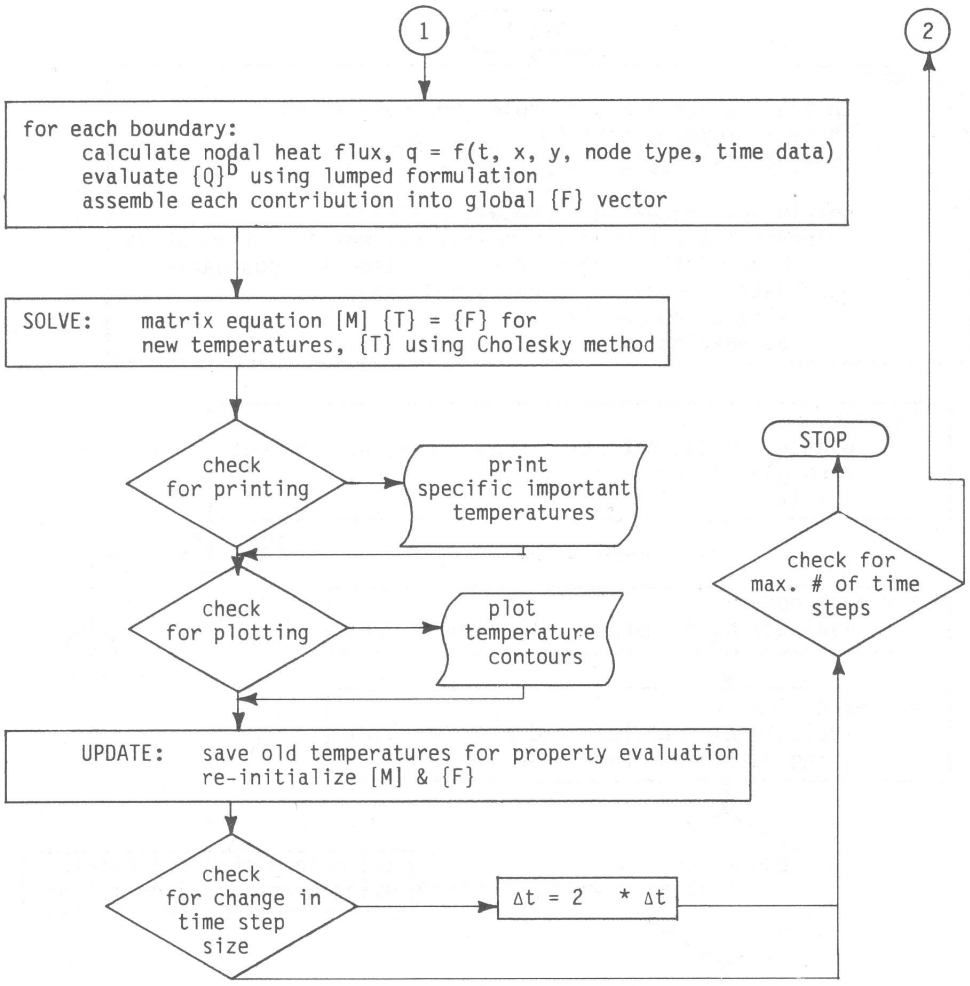

Fig. 5 Cont. — Flowchart of finite-element heat-flow model computer program.

6. Increasing the heat-transfer rate from the external surface of the mold by 10 pct produced a 5 pct decrease in solidification time.
7. Similarly, increasing thermal conductivity of the mold by 10 pct produced a 5 pct decrease in solidification time.
8. Increasing the time of air gap formation by 100 pct produced a 4 pct decrease in solidification time.
9. Increasing the initial temperature of the mold by 100 pct or increasing the initial temperature of the steel by 5 pct had little effect, increasing solidification time by less than 1 pct.

The results indicate that the model is generally insensitive to changes in these input parameters. However, it is important to model the mold geometry accurately and to use fine time steps initially. It is interesting to note that crude models may achieve acceptable accuracy using coarse, rectangular meshes and large, constant time steps initially since the errors partially offset one another.

VII. RESULTS

To demonstrate an application of the heat-transfer model, a sample simulation run was designed to follow a typical ingot completely through all stages of processing prior to rolling. A corrugated, 23,000 kg, 760 × 1520 mm (30 × 60 in.) low-carbon steel ingot was chosen to represent a typical size that could exhibit off-corner panel cracks. Figure 9 illustrates the 672-node, 1158-element mesh, based on the geometry in Figure 3, that was used to simulate thermal processing of the ingot and mold under conditions likely to produce cracks. Details of the processing conditions fed to the model in the simulation are summarized in Table I.

The run was performed using a strip time from the mold of 14,400 seconds (4 hours) and a "medium" track time of 20,700 seconds (5.75 hours) which includes an air cooling or unjacketed time of 6300 seconds (1.75 hours). This was chosen because it falls within the range of track times found to be most susceptible to the production of off-corner panel cracks.[33] The ingot then was "charged" into an initially hot (1000 °C) soaking pit which again was thought to be conducive to panel-crack formation. A "fast" reheating rate was adopted to increase the interior pit temperature linearly to a soaking temperature of 1200 °C after a high firing time of 12,700 seconds (3.53 hours). This time was determined from the practice normally employed by Stelco to calculate the time to reach the soaking pit set point temperature, as a function of track time[33]

$$t_{\text{high fire}} = 970 + 81.6\sqrt{t_{\text{track}}} \qquad [13]$$

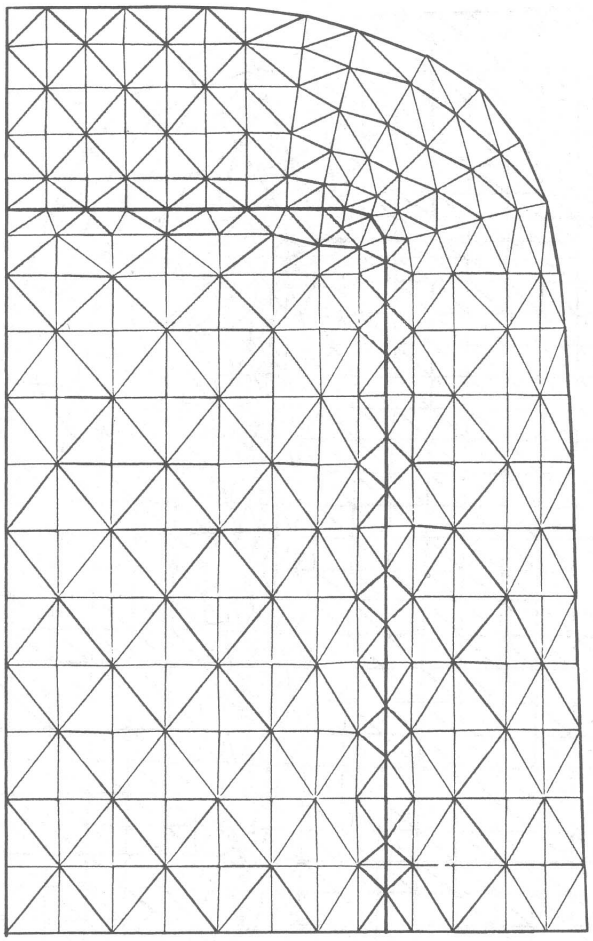

Fig. 6 — Finite-element mesh for a 230 × 405 mm ingot and mold used for comparison with industrial temperature measurements.

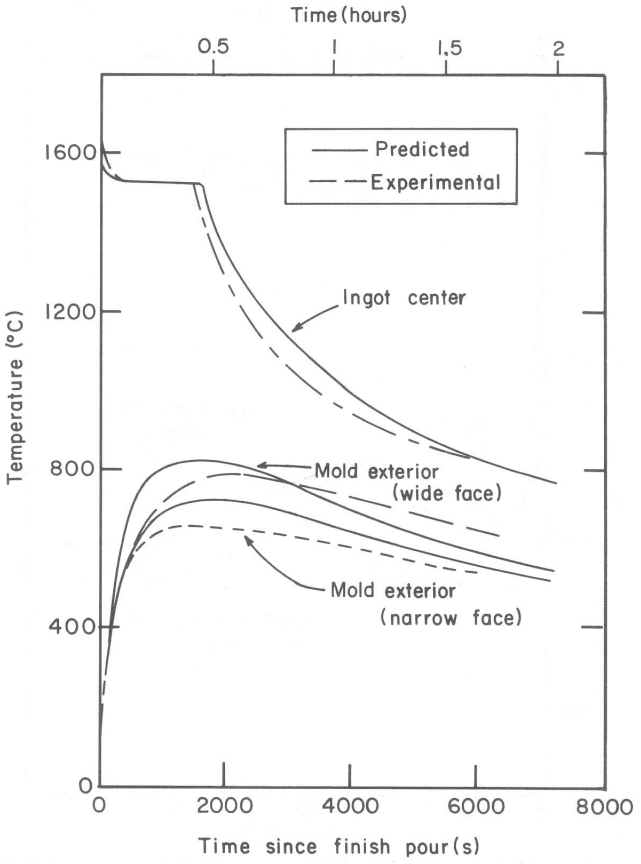

Fig. 7 — Comparison of measured and calculated temperature responses for 230 × 405 mm steel ingot.

Reheating was prolonged for 49,300 seconds (13.69 hours) until removal of the ingot from the pit at 70,000 seconds (19.44 hours). Finally, the run was continued (after drawing) to determine the thermal fields that arise during final air cooling to ambient temperature.

Figure 10 presents the temperature contours calculated by the model at various critical stages during processing of the ingot. These contours were produced using a computer program developed to draw line segments across individual elements of the finite-element mesh corresponding to the given isotherms. This was done through a simple linear interpolation of temperatures at the three nodes of each element. Figure 11 alternatively presents temperatures at several important locations in the ingot as functions of time during processing. A comparison of Figures 10(a) and (b) shows that the corner of the ingot, which cools to below

Table I. Processing Conditions Used for Model Simulation

Ingot size	760 × 1520 mm
Steel composition	low carbon steel 0.15 pct C, 1.50 pct Mn, 0.35 pct Si, 0.01 pct S, 0.01 pct P, 0.04 pct Al
Liquidus temperature	1513 °C
Solidus temperature	1486 °C
Initial steel temperature	1530 °C
Initial mold temperature	25 °C
Strip time	14,400 seconds (4 hours)
Unjacketed or air cooling time	6300 seconds (1.75 hours)
Track time	20,700 seconds (5.75 hours)
Initial soaking pit temperature	1000 °C
High firing time	12,700 seconds (3.53 hours)
Final soaking pit temperature	1200 °C
Total time reheating in pit	49,300 seconds (13.69 hours)
Draw time	70,000 seconds (19.44 hours)
Initial time step size	0.9375 seconds
Maximum time step size	30 seconds

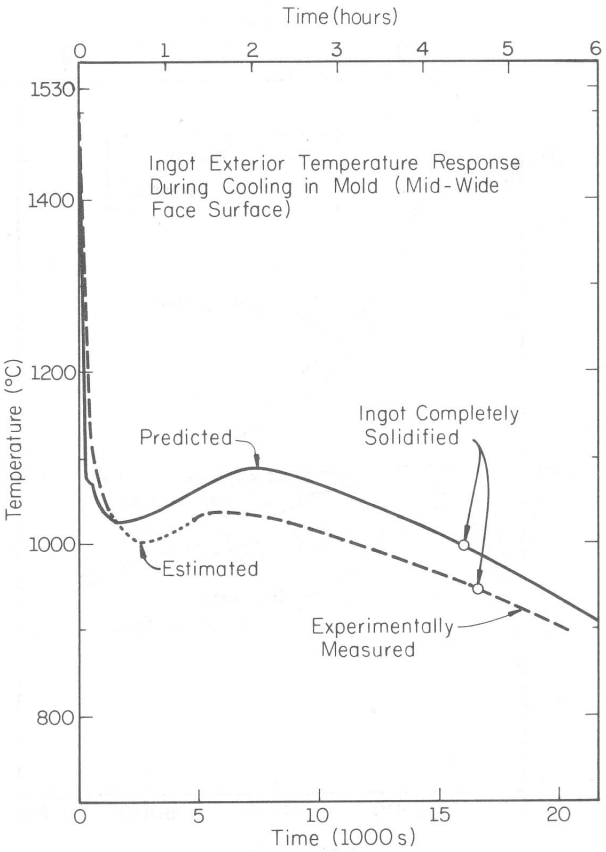

Fig. 8 — Comparison of measured and calculated temperature responses at mid-wide face surface of 870 × 1130 mm, 15,000 kg steel ingot during cooling in the mold.

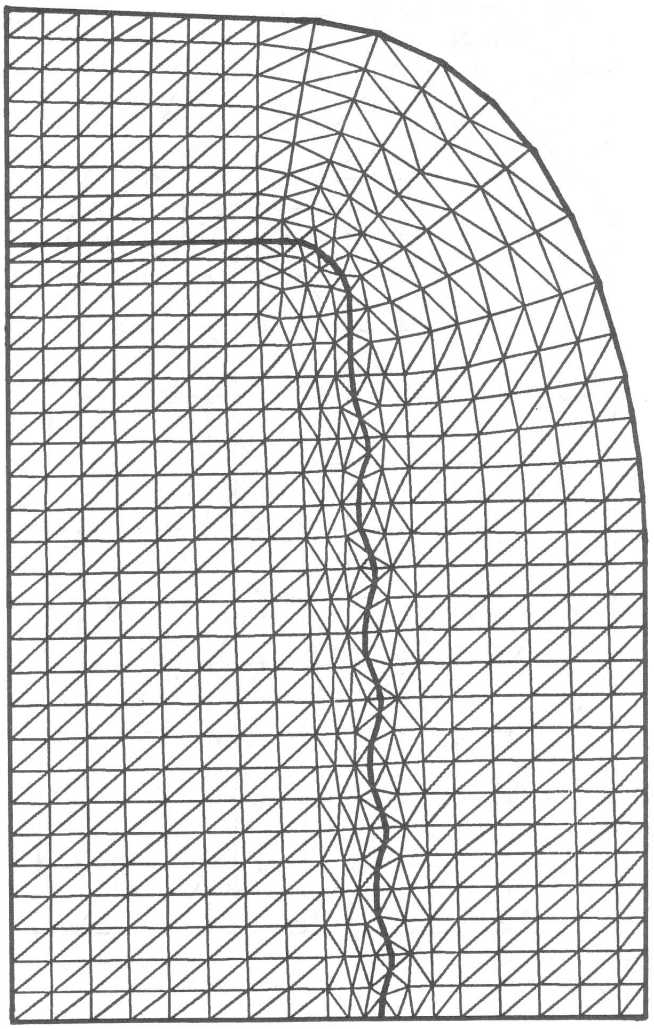

Fig. 9 — Finite-element mesh for a 760 × 1520 mm, 23,000 kg ingot and mold.

670 °C within 0.75 hour after teeming, subsequently reheats to almost 725 °C after 4 hours of cooling in the mold. This same reheating phenomenon occurs to varying extents all across the ingot surface and is illustrated more clearly in the surface temperature histories given in Figure 11. The reheating occurs partly because the inside surface of the mold, which initially acts as a heat sink quenching the ingot surface, eventually heats up and reduces heat transfer across the interface.

The ingot surface temperature does not reach a maximum and begins to decline again until thermal equilibrium is achieved with the mold interface. As seen in Figure 11, this occurs faster with increasing distance from the corner since the ingot and mold surface remain in contact longer. Heat flow across the ingot/mold gap is drastically reduced by formation of the air gap, thereby allowing heat conducted from the hot interior of the ingot to accumulate at the surface. The corner, for example, is still increasing in temperature at time of stripping.

As cooling in the mold progresses, the superheat is completely dissipated within 3600 seconds (one hour), even with no convection in the liquid. After 12,480 seconds (3.5 hours), the ingot has completely solidified. This time agrees with measurements by previous researchers.[9,15] It is interesting to note that the interior surface of the mold heats up dramatically, particularly near the center of the wide face where it reaches a maximum of over 900 °C. This high value is again in general agreement with previous measurements[15] and reflects the prolonged contact time between ingot and mold in this vicinity. By the time of stripping, 14,400 seconds (4 hours), temperature gradients within the ingot have subsided somewhat. The ingot center cools rapidly while the surface temperatures shown in Figure 11 stabilize at relatively constant values that increase with increasing distance from the corner.

Immediately after stripping, the rapid surface cooling forces the previously smooth temperature isotherms to bend sharply across the ingot surface as shown in Figure 10(c). Figure 10(d) illustrates the progress of a two-phase transformation region between the Ar_3 (780 °C) and Ar_1 (650 °C) as it moves deeper into the ingot during air cooling. By the time of charging, after 1.75 hours of air cooling, the two-phase region defines a band that corresponds approximately to the eventual location of off-corner panel cracks. The increased distance between the isotherms from Figures 10(c) to (d) shows that temperature gradients within the ingot gradually subside as air cooling progresses. Because the ingot is cooling so slowly, the heat liberated during the $\gamma \rightarrow \alpha$ phase transformation does not cause recalescence and has relatively little effect on the development of the temperature profiles.

Figure 10(e) illustrates the dramatic change in temperature distribution that occurs shortly after charging the

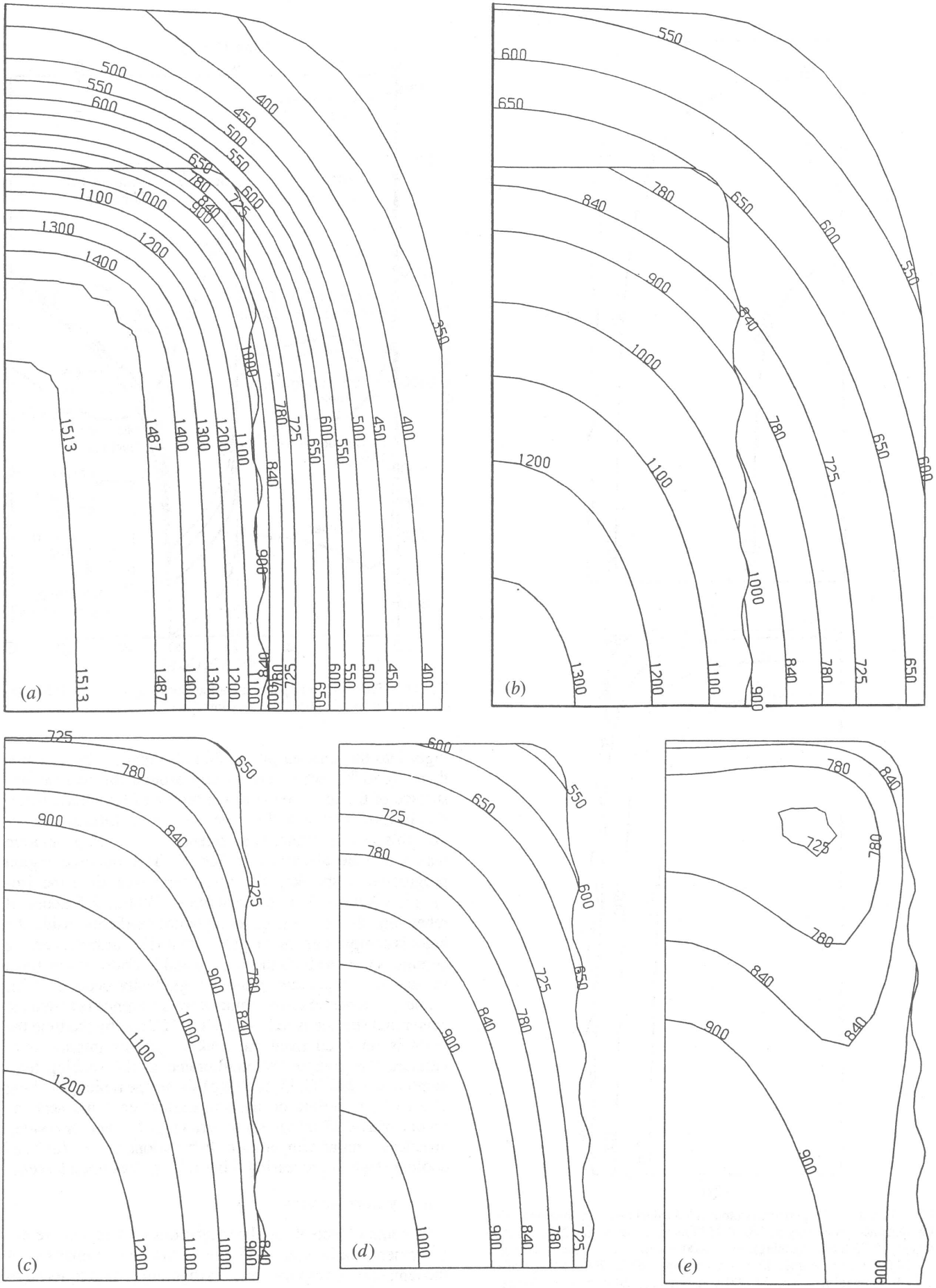

Fig. 10 — Temperature contours (°C) calculated by heat-flow model for simulated processing of 760 × 1520 mm steel ingot: (*a*) 2700 s (mold cooling, 0.75 h after teeming). (*b*) 14,400 s (strip after 4 h mold cooling). (*c*) 15,000 s (air cooling, 10 min after strip). (*d*) 20,700 s (charge after 1.75 h air cooling). (*e*) 21,900 s (reheating, 20 min after charge). (*f*) 29,700 s (reheating, 2.5 h after charge). (*g*) 70,900 s (air cooling, 15 min after draw).

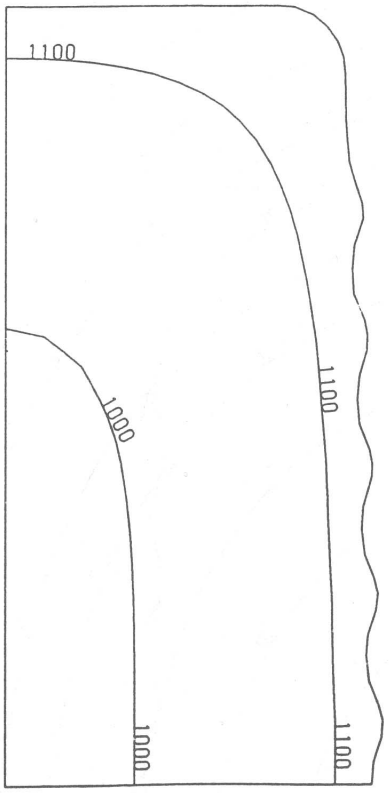

(*f*)

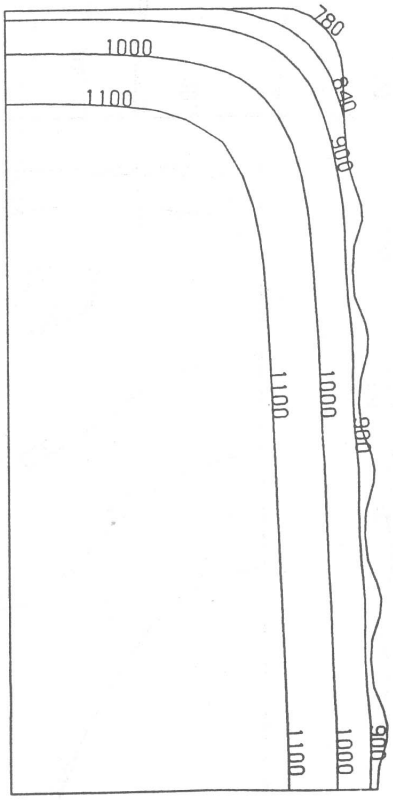

(*g*)

Fig. 10 Cont. — Temperature contours (°C) calculated by heat-flow model for simulated processing of 760 × 1520 mm steel ingot: (*a*) 2700 s (mold cooling, 0.75 h after teeming). (*b*) 14,400 s (strip after 4 h mold cooling). (*c*) 15,000 s (air cooling, 10 min after strip). (*d*) 20,700 s (charge after 1.75 h air cooling). (*e*) 21,900 s (reheating, 20 min after charge). (*f*) 29,700 s (reheating, 2.5 h after charge). (*g*) 70,900 s (air cooling, 15 min after draw).

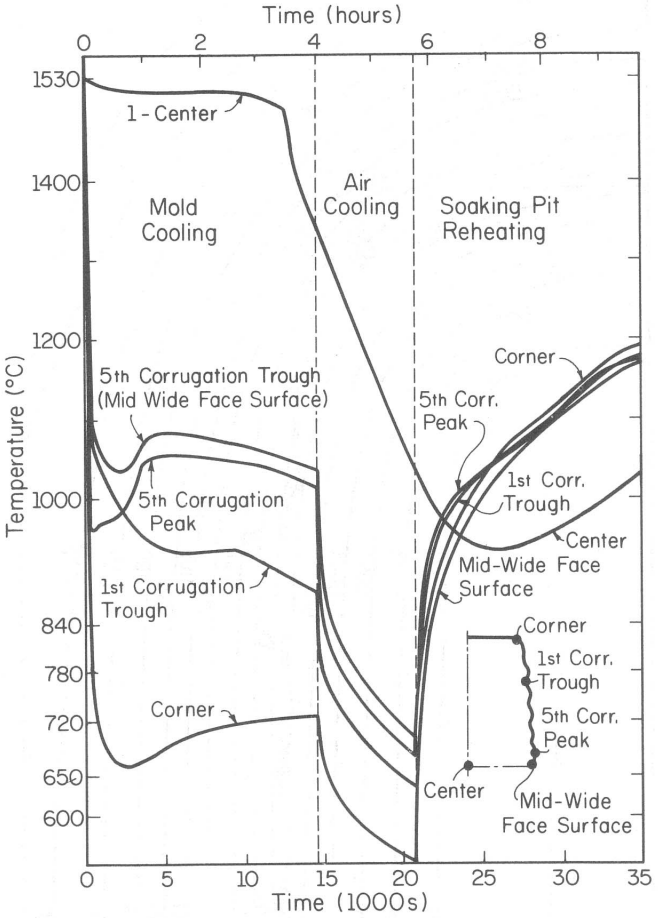

Fig. 11 — Temperature response at various locations in 760 × 1520 mm, corrugated ingot calculated by heat-flow model.

ingot into the soaking pit. Within 20 minutes, the Ac_3 isotherm (840 °C) wraps completely around the narrow-face surface of the ingot to enclose a region of two-phase material heating within a thin zone of retransformed austenite. This has important consequences for stress generation which will be discussed in Part II. The enclosed region progressively shrinks, and with increasing time the isotherms continue their redistribution. Within 2.5 hours of reheating, the reversal of temperature gradients inside the ingot is complete as shown in Figure 10(f). Further reheating continues to raise both the surface and interior temperatures as internal temperature gradients gradually decline. After 5 hours of reheating, the temperature difference between the center and surface is only about 100 °C, and by the time the ingot is removed from the soaking pit, its internal temperature has completely equilibrated at the soaking temperature of 1200 °C. Figure 10(g) shows the rapid quenching effect of air cooling on the temperature contours near the ingot surface, 15 minutes after drawing. Further air cooling produces similar temperature distributions to the first air-cooling stage of processing if hot rolling does not intervene.

Effect of Corrugations

The importance of mold corrugations on temperature development can be seen in Figure 11 through comparison of the temperature response at a corrugation peak and its adjacent trough, situated at the middle of the broad face. As expected, the corrugation peak both cools and heats more

rapidly than the trough. The greatest temperature difference between the peak and trough of a corrugation arises when temperature gradients are changing the most rapidly: over 100 °C cooler just after casting, 30 °C cooler after stripping, and 80 °C hotter soon after charging. At other times, the difference ranges from 20 °C during mold and air cooling to less than 10 °C later during reheating. However, even only 20 °C produces a distinct difference in color between corrugation peaks and troughs that is readily discernible on the ingot surface during air cooling. It is interesting to note that the corrugation peak reheats over 100 °C in the mold, compared with only 45 °C at the trough at the middle of the broad face. The isotherms in Figure 10 are smooth and virtually unaffected by the presence of corrugations. Thus, the temperature difference between the peak and trough of a corrugation arises mainly from their difference in depth or distance from the ingot centerplane.

VIII. SUMMARY

A mathematical heat-flow model has been developed to calculate the two-dimensional temperature distribution in a static-cast steel ingot from the instant of teeming until the time of hot rolling. The accuracy of the model was verified through comparison with industrial temperature measurements performed on a small, steel ingot solidifying in the mold.

A sensitivity analysis of the heat-flow model demonstrated the importance of correctly modeling the exact geometry of the mold. In particular, inclusion of rounded corners is very important for reliably predicting temperatures in a solidifying ingot. A method to calculate the time of air gap formation as a function of position along the ingot/mold interface was incorporated into the model. Although this function was found to have only a minor effect on solidification time in a small ingot, it undoubtedly has a more important effect on temperature in larger ingot sizes which have much longer gap formation times.

Finally, the model was employed to simulate temperature development in a 760 × 1520 mm, corrugated, low-carbon steel ingot during the various processing stages prior to hot rolling. Because the analysis was performed using the finite-element method, the results can easily be input to a finite-element, thermal stress model using the same mesh geometry. In addition, several interesting features regarding temperature development in steel ingot processing were observed:

1. The surface of the ingot reheats significantly while cooling in the mold.
2. The presence of mold corrugations, while not significantly influencing overall heat-transfer rates, does produce local variations in temperature in the order of 30 °C.
3. The early stages of reheating in the soaking pit produce drastic changes in the generally smooth, elliptical temperature contours as the temperature gradients reverse direction. Of particular interest is the development of a transient region within the ingot, potentially composed of two-phase material, that is surrounded by steel at higher temperatures. This will have important consequences for stress generation and, ultimately, for panel crack formation.

NOMENCLATURE

C_p	Specific heat (J kg^{-1} °C^{-1})
d	Distance along ingot surface from corner (m)
H	Enthalpy (J kg^{-1})
h_{cond}	Conductive heat transfer coefficient (W m^{-2} °C^{-1})
k	Thermal conductivity (W m^{-1} °C^{-1})
q	Heat flux (W m^{-2})
T	Temperature (°C)
T_{LIQ}	Liquidus temperature (°C)
T_{SOL}	Solidus temperature (°C)
T_{SI}	Surface temperature of ingot (°C)
T_{SM}	Surface temperature of mold (°C)
T_{PIT}	Average internal soaking pit temperature (°C)
T_∞	Ambient temperature (°C)
t	Time (s)
t_{gap}	Ingot/mold air gap formation time (s)
t_{strip}	Time of stripping ingot from mold (s)
t_{track}	Time of charging ingot to soaking pit (s)
$t_{high\ fire}$	Duration of high firing rate in soaking pit (s)
t_{draw}	Time of ingot removal from soaking pit (s)
Δt	Time step size (s)
x, y	Coordinate directions (m)
$[k]^e$	3 × 3 element conductivity matrix
$[c]^e$	3 × 3 element capacitance matrix
$\{\mathbf{F}\}$	Global thermal force vector
$\{\mathbf{Q}\}^b$	2 × 1 element boundary heat flux vector
$\bar{\varepsilon}$	Effective emissivity
ε_I	Emissivity of ingot surface
ε_M	Emissivity of mold surface
ρ	Density (kg m^{-3})
σ	Stefan-Boltzmann radiation constant (5.67 × 10^{-8} W m^{-2} °K^{-4})

ACKNOWLEDGMENTS

The authors wish to thank Stelco, Inc. both for support of research expenses and the provision of valuable data, and the Natural Sciences and Engineering Research Council of Canada, and Noranda for support of BGT.

REFERENCES

1. B. G. Thomas, J. K. Brimacombe, and I. V. Samarasekera: *ISS Transactions*, 1986, vol. 7, pp. 7-20.
2. B. G. Thomas, J. K. Brimacombe, and I. V. Samarasekera: *ISS Transactions*, 1986, vol. 7, pp. 21-29.
3. R. J. Sarjant and M. R. Slack: *J. Iron Steel Inst.*, 1954, vol. 177, pp. 428-44.
4. E. Y. Kung, J. R. Dahm, and G. B. DeLancey: (J and L Steel), *Instrument Society of America Annual Conference L.A.*, 1967, vol. 6, No. 2, pp. 162-68.
5. R. Severin: *Mathematical Models in Metallurgical Process Development*, Iron and Steel Inst., London, 1970, pp. 147-61.
6. T. Mori and K. Narita: *ISIJ Trans.*, 1972, vol. 12, pp. 83-90.
7. I. D. Massey and A. T. Sheridan: *J. Iron Steel Inst.*, May 1971, pp. 391-96.
8. R. Severin and R. Pesch: *Stahl und Eisen,* 1973, vol. 93, No. 18, B.I.S.I. No. 11901, pp. 834-37.
9. H. W. den Hartog, J. M. Rabenberg, and J. Willemse: *Ironmaking and Steelmaking*, 1975, vol. 2, pp. 134-44.
10. S. D. Cumming: *J. of Australasian Institute of Metals*, March 1977, vol. 22, No. 1, pp. 11-16.
11. Kawasaki Steel Corporation: "On the Three Dimensional Simulation Model for Ingot Solidification and Heating in Soaking Pit", May 1979.

12. I. Ohnaka and T. Fukasako: *ISIJ Trans.*, 1981, vol. 21, pp. 485-94.
13. K. Tashiro, S. Watanabe, I. Kitagawa, and I. Tamura: *ISIJ Trans.*, 1983, vol. 23, pp. 312-21.
14. H. J. Schulze and P. M. Beckett: *Proc. R. Soc.*, London, Series A, February 8, 1983, vol. 385, pp. 313-43.
15. M. R. Ozgu, D. H. Bright, and D. K. Watkins: *Steelmaking Proc.*, ISS, 1985, vol. 68, pp. 315-29.
16. *Physical Constants of Some Commercial Steels at Elevated Temperatures*, B. I. S. R. A., ed., Butterworths, London, 1953, pp. 1-38.
17. *Thermophysical Properties of Matter, the TPRC Data Series: A Comprehensive Compilation of Data*, Y. S. Touloukian, ed., New York, NY, IFI/Plenum, 1970, vols. 1, 4, 7, 10.
18. P. J. Wray: *Modelling of Casting and Welding Processes*, AIME Conference Proceedings, 1980, pp. 247-57.
19. J. Ormerod, R. Taylor, and R. J. Edwards: *Metals Technology*, April 1978, pp. 109-13.
20. F. Baitler: *La Commission de l'acierie du UDE*, No. 447.
21. Y. Dardel: *Editions de la Revue de Metallurgie*, Paris, 1964, pp. 1-266.
22. *Chemical Engineer's Handbook*, 5th ed., R. H. Perry and C. H. Chilton, eds., McGraw-Hill, New York, NY, 1973, pp. 10-11.
23. V. A. Diener, A. Drastik, and W. Haumann: *Archive für das Eisenhüttenwesen*, July 1972, vol. 43, No. 7, pp. 525-33.
24. F. Kavicka: *Slevarenstvi*, B.I.S.I. 15540, 1976, vol. 24, No. 11, pp. 448-52.
25. F. Oeters, K. Ruttiger, and H. J. Selenz: *Casting and Solidification of Steel*, 1977, pp. 125-67.
26. J. Szekely and N. J. Themelis: *Rate Phenomena in Process Metallurgy*, Wiley Interscience, New York, NY, 1971, pp. 288-89.
27. B. G. Thomas: Ph.D. Thesis, University of British Columbia, Vancouver, BC, Canada, 1985.
28. B. G. Thomas, I. V. Samarasekera, and J. K. Brimacombe: *Metall. Trans. B*, 1984, vol. 15B, pp. 307-18.
29. I. Ohnaka and T. Fukasako: *Trans. Iron Steel Inst. Japan*, 1977, vol. 17, pp. 410-18.
30. T. Dupont, G. Fairweather, and J. Johnson: *Siam J. Numerical Analysis*, 1974, vol. 11, pp. 392-410.
31. M. Hogge: *Numerical Methods in Heat Transfer*, R. Lewis, K. Morgan, and O. C. Zienkiewicz., eds., John Wiley and Sons, Ltd., 1981, pp. 75-90.
32. E. Lemmon: *Numerical Methods in Heat Transfer*, R. Lewis, K. Morgan, and O. C. Zienkiewicz, eds., John Wiley and Sons, Ltd., New York, NY, 1981, pp. 201-13.
33. J. E. Lait: Stelco, Inc., Hamilton, ON, Canada, private communication, 1984.
34. K. F. Behrens and H. Weingart: *Stahl und Eisen*, 1969, vol. 89, pp. 1457-67.